Available online at www.sciencedirect.com
SCIENCE DIRECT®
International Journal of Solids and Structures 42 (2005) 4239–4257
INTERNATIONAL JOURNAL OF SOLIDS and STRUCTURES
www.elsevier.com/locate/ijsolstr

Three-dimensional analysis of the coupled thermo-piezoelectro-mechanical behaviour of multilayered plates using the differential quadrature technique

K.M. Liew [a,b,*], Jordan Z. Zhang [a], C. Li [b], S.A. Meguid [c]

[a] *Nanyang Centre for Supercomputing and Visualisation, Nanyang Technological University, 50 Nanyang Avenue, Singapore 639798, Singapore*
[b] *School of Mechanical and Production Engineering, Nanyang Technological University, 50 Nanyang Avenue, Singapore 639798, Singapore*
[c] *Department of Mechanical and Industrial Engineering, University of Toronto, 5 King's College Road, Toronto, Ont., Canada M5S 3G8*

Received 8 March 2004; received in revised form 22 December 2004

Abstract

This paper investigates the behaviour of multilayered composite plates subject to thermo-piezoelectric-mechanical loading. The analysis is performed using the three-dimensional equations of thermo-piezoelasticity and the differential quadrature (DQ) numerical technique. Solutions to the thermo-piezoelectric laminated plates are made possible with the development and implementation of a DQ layerwise modelling technique. The formulation allows different boundary conditions to be imposed at the edges of the plate. Numerical results for different example plate problems are presented, and the effects of the thermo-piezoelasticity and boundary conditions of these problems are investigated. The DQ model predictions are validated with existing results as the comparison reveals good agreement between two.

Keywords: Three-dimensional analysis; Differential quadrature method; Layerwise model; Thermo-piezoelectric-elasticity

* Corresponding author. Address: School of Mechanical and Production Engineering, Nanyang Technological University, 50 Nanyang Avenue, Singapore 639798, Singapore. Tel.: +65 6790 4076; fax: +65 6793 6763.
E-mail address: mkmliew@ntu.edu.sg (K.M. Liew).

0020-7683/$ - see front matter
doi:10.1016/j.ijsolstr.2004.12.018

1. Introduction

Piezoelectricity is the phenomenon whereby electric polarization is developed in deformed materials. The effect of electro-mechanical coupling in such materials has immense potential in engineering applications. A good example is the use of this class of materials as sensors and actuators in micro-electro-mechanical systems (MEMS), for instance, the piezoelectric accelerometer which triggers an airbag in ten thousandths of a second during an accident.

With the advent of a new generation of electronic devices, their reliability and integrity are essential for safe operation. In addition, because these devices are designed to operate under various electro-thermo-mechanical conditions over a broad spectrum, their design and manufacturing represents a great challenge in engineering. In view of its versatility and importance to engineering applications, we devote our attention to a multilayered piezoelectric medium. In this case, a stack of materials is laminated in different orientations as a multifunctional unit that can be used as a sensor of the induced electric field as a result of thermo-mechanical strain field, or as an actuator that introduces thermo-mechanical strains for a given electric field. This self-monitoring and self-controlling device has numerous potential applications in industry.

General theories of laminated composite plates can be found in Reddy (2004). Among the early investigations of multilayered structures is the work of Tiersten (1971), in which the governing differential equations for a thermo-piezoelectric medium that is interacting with an electric field are derived. Thereafter, Mindlin (1974) deduced equations that described small vibrations of piezoelectric plates, including the coupling between the deformation, temperature and electric fields. Nowacki (1978) provided a uniqueness theorem for the solution of the three-dimensional equations of thermo-piezoelectricity. Ray et al. (1992, 1993) presented three-dimensional exact solutions of simply-supported single layer and laminated flat panels with distributed actuators under transverse pressure. Three-dimensional exact solutions of simply-supported rectangular plates coupled with distributed sensors and actuators were also reported by Heyliger (1994) and Dube et al. (1996). Furthermore, Xu et al. (1995) and Heyliger (1997) developed 3D analytical solutions for multilayered piezoelectric plates to study their electro-elastic response. However, all of these studies only apply to simply-supported plates. Vel and Batra (2000, 2003) recently developed a three-dimensional analytical solution in terms of an infinite series for the thermo-piezoelectric deformations of laminated thick plates with various support edges.

We extend the differential quadrature method (Bert and Malik, 1996; Liew et al., 1996a,b; Han and Liew, 1997a,b,c; Liew and Han, 1997; Liew and Teo, 1998; Liu and Liew, 1998a,b; Liew and Teo, 1999; Liu and Liew, 1999a,b; Teo and Liew, 1999a,b; Liew and Liu, 2000; Liew et al., 2001) into a three-dimensional coupled layerwise thermo-piezoelastic model. The method is appealing because of its robustness and ease of implementation. It is particularly suitable for higher-order interpolation and element-free discretisation. The principle and procedures of the DQ method are detailed in Zhang et al. (2003). The selection of reasonable spacing patterns of grid points is crucial for obtaining accurate solutions. In this study, a symmetrically cosine spacing of grid points, given by

$$x_i = \frac{1 - \cos\frac{i-1}{N_g - 1}\pi}{2} \quad i = 1, 2, \ldots, N_g \tag{1}$$

is used for discretization, where N_g is the number of discrete grid points. Liew et al. (1999) numerically verified the strong stability and rapid convergence of the DQ method with cosine spacing. We present a layerwise differential quadrature method (Liew et al., 2004) for the analysis of thermo-piezoelastic multilayered composite plates.

2. Layerwise theory for three-dimensional thermo-piezoelasticity

Srinivas and Rao (1970) and Pagano (1970) studied laminated structures from the three-dimensional viewpoint. In recent years, the same approach was successfully applied to analyse the performance of laminated structures with various boundary conditions using the differential quadrature method (Liew et al., 2002). We extend the earlier formulations to treat the current thermo-piezoelastic layered medium.

2.1. Governing equations of the thermo-piezoelectric-elastic medium

The equilibrium equations for a thermo-piezoelastic medium can be given as (Nowacki, 1975):

$$\frac{\partial \sigma_x}{\partial x}+\frac{\partial \tau_{xy}}{\partial y}+\frac{\partial \tau_{xz}}{\partial z}=0,\quad \frac{\partial \tau_{xy}}{\partial x}+\frac{\partial \sigma_y}{\partial y}+\frac{\partial \tau_{yz}}{\partial z}=0,\quad \frac{\partial \tau_{zx}}{\partial x}+\frac{\partial \tau_{yz}}{\partial y}+\frac{\partial \sigma_z}{\partial z}=0 \tag{2}$$

$$\frac{\partial D_x}{\partial x}+\frac{\partial D_y}{\partial y}+\frac{\partial D_z}{\partial z}=0 \tag{3}$$

$$\lambda_x\frac{\partial^2 T}{\partial x^2}+\lambda_y\frac{\partial^2 T}{\partial y^2}+\lambda_z\frac{\partial^2 T}{\partial z^2}=0 \tag{4}$$

where σ_x, σ_y and σ_z are normal stresses, τ_{xy}, τ_{xz} and τ_{yz} are shear stresses, D_i's ($i=x$, y, and z) are electric displacement vectors, λ_i's ($i=x$, y, and z) are thermal conductivity and T is temperature.

For a homogeneous, orthotropic thermo-piezoelastic material, the linear constitutive equations are

$$\begin{Bmatrix}\sigma_x\\ \sigma_y\\ \sigma_z\\ \tau_{yz}\\ \tau_{zx}\\ \tau_{xy}\end{Bmatrix}=\begin{bmatrix}C_{11}&C_{12}&C_{13}&0&0&0\\ C_{12}&C_{22}&C_{23}&0&0&0\\ C_{13}&C_{23}&C_{33}&0&0&0\\ 0&0&0&C_{44}&0&0\\ 0&0&0&0&C_{55}&0\\ 0&0&0&0&0&C_{66}\end{bmatrix}\cdot\begin{Bmatrix}\varepsilon_x\\ \varepsilon_y\\ \varepsilon_z\\ \gamma_{yz}\\ \gamma_{zx}\\ \gamma_{xy}\end{Bmatrix}-\begin{bmatrix}0&0&e_1\\ 0&0&e_2\\ 0&0&e_3\\ 0&e_4&0\\ e_5&0&0\\ 0&0&0\end{bmatrix}\cdot\begin{Bmatrix}E_x\\ E_y\\ E_z\end{Bmatrix}-\begin{bmatrix}\beta_1\\ \beta_2\\ \beta_3\\ 0\\ 0\\ 0\end{bmatrix}T \tag{5}$$

and

$$\begin{Bmatrix}D_x\\ D_y\\ D_z\end{Bmatrix}=\begin{bmatrix}0&0&0&0&e_5&0\\ 0&0&0&e_4&0&0\\ e_1&e_2&e_3&0&0&0\end{bmatrix}\cdot\begin{Bmatrix}\varepsilon_x\\ \varepsilon_y\\ \varepsilon_z\\ \gamma_{yz}\\ \gamma_{zx}\\ \gamma_{xy}\end{Bmatrix}+\begin{bmatrix}\eta_1&0&0\\ 0&\eta_2&0\\ 0&0&\eta_3\end{bmatrix}\cdot\begin{Bmatrix}E_x\\ E_y\\ E_z\end{Bmatrix}+\begin{bmatrix}0\\ 0\\ p_3\end{bmatrix}T \tag{6}$$

where C_{ij}, e_i, η_i, β_i and p_3 denote the matrices of elastic constants, piezoelectric constants, dielectric constants, stress-temperature coefficients and pyroelectric constants of the thermo-piezoelastic material, respectively. These properties are assumed to be temperature independent.

2.2. Simplified governing equations for cylindrical bending

Consider a laminated plate (Fig. 1) made from orthotropic piezoelastic material with uniform thickness H, width a and infinite length in y-direction. This can be treated as a plane strain problem, and all entities become independent of y.

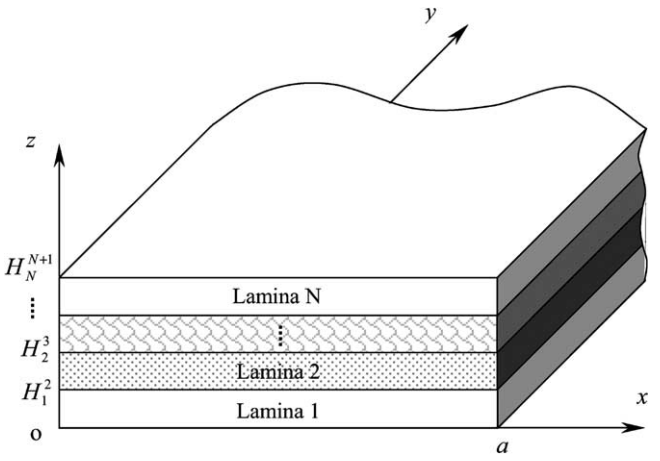

Fig. 1. A homogeneous/laminated piezoelectric plate.

The kinematic relations are

$$\varepsilon_x = \frac{\partial u}{\partial x}, \quad \varepsilon_z = \frac{\partial w}{\partial z}, \quad \gamma_{xz} = \frac{\partial u}{\partial z} + \frac{\partial w}{\partial x}, \text{ and } \varepsilon_y = \gamma_{yz} = \gamma_{xy} = 0 \tag{7}$$

Introducing the electric potential ϕ then

$$E_x = -\frac{\partial \phi}{\partial x}, \quad E_z = -\frac{\partial \phi}{\partial z} \text{ and } E_y = 0 \tag{8}$$

Substitute Eqs. (7) and (8) into Eqs. (5) and (6), and we have

$$\tau_{yz} = \tau_{xy} = 0 \text{ and } D_y = 0 \tag{9}$$

$$\begin{aligned} \sigma_x &= C_{11}\frac{\partial u}{\partial x} + C_{13}\frac{\partial w}{\partial z} + e_1\frac{\partial \phi}{\partial z} - \beta_1 T, \quad \sigma_y = C_{12}\frac{\partial u}{\partial x} + C_{23}\frac{\partial w}{\partial z} + e_2\frac{\partial \phi}{\partial z} - \beta_2 T \\ \sigma_z &= C_{13}\frac{\partial u}{\partial x} + C_{33}\frac{\partial w}{\partial z} + e_3\frac{\partial \phi}{\partial z} - \beta_3 T, \quad \tau_{zx} = C_{55}\left(\frac{\partial u}{\partial z} + \frac{\partial w}{\partial x}\right) + e_5\frac{\partial \phi}{\partial x} \end{aligned} \tag{10}$$

and

$$D_x = e_5\left(\frac{\partial u}{\partial z} + \frac{\partial w}{\partial x}\right) - \eta_1\frac{\partial \phi}{\partial x}, \quad D_z = e_1\frac{\partial u}{\partial x} + e_3\frac{\partial w}{\partial z} - \eta_3\frac{\partial \phi}{\partial z} + p_3 T \tag{11}$$

Further, substituting Eqs. (9)–(11) into Eqs. (2)–(4) and considering the plane strain condition, the governing equations becomes

$$C_{11}\frac{\partial^2 u}{\partial x^2} + C_{55}\frac{\partial^2 u}{\partial z^2} + (C_{13} + C_{55})\frac{\partial^2 w}{\partial x \partial z} + (e_1 + e_5)\frac{\partial^2 \phi}{\partial x \partial z} - \beta_1\frac{\partial T}{\partial x} = 0 \tag{12}$$

$$(C_{55} + C_{13})\frac{\partial^2 u}{\partial x \partial z} + C_{55}\frac{\partial^2 w}{\partial x^2} + C_{33}\frac{\partial^2 w}{\partial z^2} + e_5\frac{\partial^2 \phi}{\partial x^2} + e_3\frac{\partial^2 \phi}{\partial z^2} - \beta_3\frac{\partial T}{\partial z} = 0 \tag{13}$$

$$(e_5 + e_1)\frac{\partial^2 u}{\partial x \partial z} + e_5\frac{\partial^2 w}{\partial x^2} + e_3\frac{\partial^2 w}{\partial z^2} - \eta_1\frac{\partial^2 \phi}{\partial x^2} - \eta_3\frac{\partial^2 \phi}{\partial z^2} + p_3\frac{\partial T}{\partial z} = 0 \tag{14}$$

$$\lambda_x \frac{\partial^2 T}{\partial x^2} + \lambda_z \frac{\partial^2 T}{\partial z^2} = 0 \tag{15}$$

Here Eqs. (12) and (13) are the equilibrium equations, Eq. (14) is the electrostatic equation, and Eq. (15) is the heat conduction equation, which is uncoupled from the mechanical problem.

2.3. Interfacial conditions

For perfectly bounded laminates, the temperature, displacement field, surface tractions, electric potential, normal components of the electric displacement and the heat flux at the interface are continuous, i.e.,

$$[[u, w]] = 0 \text{ and } [[\sigma_z, \tau_{xz}, \tau_{yz}]] = 0 \text{ at } z = H_i^{i+1} \tag{16}$$

$$[[\phi]] = 0 \text{ and } [[D_z]] = 0 \text{ at } z = H_i^{i+1} \tag{17}$$

$$[[T]] = 0 \text{ and } [[q_z]] = 0 \text{ at } z = H_i^{i+1} \tag{18}$$

where $[[\,]]$ denotes the jump across an interface, the heat flux $q_i = -\kappa_{ij} \frac{\partial T}{\partial x_j}$ with κ_{ij} being the thermal conductivity, and H_i^{i+1} is the thickness coordinate at the surface between the ith and $i+1$th lamina. The boundary conditions to be employed for each plate case will be specified later for each plate example considered.

2.4. Differential quadrature discretisation

The principle of the DQ method is that the partial derivative of a function can be described by the function at all discrete points in the domain such that

Table 1
Convergence of present modeling and comparison with the reference exact solutions ($\bar{w} = \frac{100w}{|d_1|\phi_0}$, $\bar{\phi} = \frac{\phi}{\phi_0}$, $\bar{\sigma}_x = \frac{s^2 H \sigma_x}{Y_x |d_1| \phi_0}$, $\bar{\sigma}_y = \frac{H\sigma_y}{Y_x |d_1| \phi_0}$, where s, Y_x, α_x and d_1 are ratio of a/h, Young's modulous, thermal expansion coefficient and piezoelectric coefficient in x-direction)

a/H	Mesh	$\bar{w}$			$\bar{\sigma}_x$			$\bar{\sigma}_y$		$\bar{\phi}$
		$z=0$	$z=H/2$	$z=H$	$z=0$	$z=H/2$	$z=H$	$z=0$	$z=H$	$z=H/2$
100	7	287.54	199.90	112.25	−29.24	19.84	−29.25	−1.00	−1.002	0.499
	9	287.63	199.95	112.25	−6.278	3.138	−6.279	−1.00	−1.001	0.499
	11	287.63	199.95	112.25	−6.280	3.133	−6.280	−1.00	−1.001	0.499
	13	287.63	199.95	112.25	−6.278	3.138	−6.279	−1.00	−1.001	0.499
Dube et al. (1996)		287.6	200.0	112.3	−6.277	3.139	−6.278	−1.00	−1.001	0.499
10	7	284.92	198.24	109.64	−6.430	2.859	−6.541	−1.017	−1.061	0.494
	9	285.01	198.29	109.65	−6.206	3.092	−6.276	−1.016	−1.060	0.494
	11	285.01	198.29	109.65	−6.206	3.092	−6.276	−1.016	−1.060	0.494
	13	285.01	198.29	109.65	−6.206	3.092	−6.276	−1.016	−1.060	0.494
Dube et al. (1996)		285.1	198.4	109.8	−6.205	3.100	−6.260	−1.016	−1.060	0.494
6	7	280.30	195.33	105.12	−6.158	2.924	−6.358	−1.044	−1.167	0.485
	9	280.38	195.38	105.12	−6.081	3.011	−6.272	−1.043	−1.166	0.485
	11	280.38	195.38	105.12	−6.081	3.011	−6.272	−1.043	−1.166	0.485
	13	280.38	195.38	105.12	−6.081	3.011	−6.272	−1.043	−1.166	0.485
Dube et al. (1996)		280.7	195.7	105.4	−6.079	3.031	−6.229	−1.043	−1.166	0.485

$$f'(x_i) \cong \sum_{j=1}^{N_g} A_{ij} f(x_j) \quad i = 1, 2, \ldots, N_g \tag{19}$$

where $f(x)$ is any smooth function, f' is its derivative, N_g is the number of discrete grid points and A_{ij} is the weighting coefficient, which can be analytically determined. Adopting the principle of the DQ method, we can obtain:

$$\begin{aligned}
&\frac{\partial u_{[k,r]}}{\partial x} = \frac{\partial u(x_k, z_r)}{\partial x} = \sum_{j=1}^{J} A_{kj}^{[1]} u(x_j, z_r), \quad \frac{\partial u_{[k,r]}}{\partial z} = \frac{\partial u(x_k, z_r)}{\partial z} = \sum_{f=1}^{F_z^{\{i\}}} B_{rf}^{[1]} u(x_k, z_f) \\
&\frac{\partial w_{[k,r]}}{\partial x} = \frac{\partial w(x_k, z_r)}{\partial x} = \sum_{j=1}^{J} A_{kj}^{[1]} w(x_j, z_r), \quad \frac{\partial w_{[k,r]}}{\partial z} = \frac{\partial w(x_k, z_r)}{\partial z} = \sum_{f=1}^{F_z^{\{i\}}} B_{rf}^{[1]} w(x_k, z_f) \\
&\frac{\partial \phi_{[k,r]}}{\partial x} = \frac{\partial \phi(x_k, z_r)}{\partial x} = \sum_{j=1}^{J} A_{kj}^{[1]} \phi(x_j, z_r), \quad \frac{\partial \phi_{[k,r]}}{\partial z} = \frac{\partial \phi(x_k, z_r)}{\partial z} = \sum_{f=1}^{F_z^{\{i\}}} B_{rf}^{[1]} \phi(x_k, z_f) \\
&\frac{\partial T_{[k,r]}}{\partial x} = \frac{\partial T(x_k, z_r)}{\partial x} = \sum_{j=1}^{J} A_{kj}^{[1]} T(x_j, z_r), \quad \frac{\partial T_{[k,r]}}{\partial z} = \frac{\partial T(x_k, z_r)}{\partial z} = \sum_{f=1}^{F_z^{\{i\}}} B_{rf}^{[1]} T(x_k, z_f)
\end{aligned} \tag{20}$$

$$\begin{aligned}
&\frac{\partial^2 u_{[k,r]}}{\partial x^2} = \frac{\partial^2 u(x_k, z_r)}{\partial x^2} = \sum_{j=1}^{J} A_{kj}^{[2]} u(x_j, z_r), \quad \frac{\partial^2 u_{[k,r]}}{\partial z^2} = \frac{\partial^2 u(x_k, z_r)}{\partial z^2} = \sum_{f=1}^{F_z^{\{i\}}} B_{rf}^{[2]} u(x_k, z_f) \\
&\frac{\partial^2 w_{[k,r]}}{\partial x^2} = \frac{\partial^2 w(x_k, z_r)}{\partial x^2} = \sum_{j=1}^{J} A_{kj}^{[2]} w(x_j, z_r), \quad \frac{\partial^2 w_{[k,r]}}{\partial z^2} = \frac{\partial^2 w(x_k, z_r)}{\partial z^2} = \sum_{f=1}^{F_z^{\{i\}}} B_{rf}^{[2]} w(x_k, z_f) \\
&\frac{\partial^2 \phi_{[k,r]}}{\partial x^2} = \frac{\partial^2 \phi(x_k, z_r)}{\partial x^2} = \sum_{j=1}^{J} A_{kj}^{[2]} \phi(x_j, z_r), \quad \frac{\partial^2 \phi_{[k,r]}}{\partial z^2} = \frac{\partial^2 \phi(x_k, z_r)}{\partial z^2} = \sum_{f=1}^{F_z^{\{i\}}} B_{rf}^{[2]} \phi(x_k, z_f) \\
&\frac{\partial^2 T_{[k,r]}}{\partial x^2} = \frac{\partial^2 T(x_k, z_r)}{\partial x^2} = \sum_{j=1}^{J} A_{kj}^{[2]} T(x_j, z_r), \quad \frac{\partial^2 T_{[k,r]}}{\partial z^2} = \frac{\partial^2 T(x_k, z_r)}{\partial z^2} = \sum_{f=1}^{F_z^{\{i\}}} B_{rf}^{[2]} T(x_k, z_f)
\end{aligned} \tag{21}$$

$$\begin{aligned}
&\frac{\partial^2 u_{[k,r]}}{\partial x \partial z} = \frac{\partial^2 u(x_k, z_r)}{\partial x \partial z} = \sum_{j=1}^{J} A_{kj}^{[1]} \cdot \sum_{f=1}^{F_z^{\{i\}}} B_{rf}^{[1]} u(x_j, z_f) \\
&\frac{\partial^2 w_{[k,r]}}{\partial x \partial z} = \frac{\partial^2 w(x_k, z_r)}{\partial x \partial z} = \sum_{j=1}^{J} A_{kj}^{[1]} \cdot \sum_{f=1}^{F_z^{\{i\}}} B_{rf}^{[1]} w(x_j, z_f) \\
&\frac{\partial^2 \phi_{[k,r]}}{\partial x \partial z} = \frac{\partial^2 \phi(x_k, z_r)}{\partial x \partial z} = \sum_{j=1}^{J} A_{kj}^{[1]} \cdot \sum_{f=1}^{F_z^{\{i\}}} B_{rf}^{[1]} \phi(x_j, z_f)
\end{aligned} \tag{22}$$

where i ($i = 1, 2, \ldots, N_L$) refers to the sequence number of laminae, and N_L is the total number of laminae. A and B's are the weighting coefficients in the respective x and z-directions. In these formulations, the superscript indicates the order of derivative and the subscript refers to the grid points. J and $F_z^{\{i\}}$ are the number of the grid points in the x and z-directions within the ith layer. With these expressions, the governing equations in (12)–(15) can be discretised as

$$
\begin{aligned}
&C_{11}^{\{i\}}\frac{\partial^2 u_{[k,r]}}{\partial x^2}+C_{55}^{\{i\}}\frac{\partial^2 u_{[k,r]}}{\partial z^2}+\left(C_{13}^{\{i\}}+C_{55}^{\{i\}}\right)\frac{\partial^2 w_{[k,r]}}{\partial x\partial z}+\left(e_1^{\{i\}}+e_5^{\{i\}}\right)\frac{\partial^2 \phi_{[k,r]}}{\partial x\partial z}-\beta_1^{\{i\}}\frac{\partial T_{[k,r]}}{\partial x}=0\\
&\left(C_{55}^{\{i\}}+C_{13}^{\{i\}}\right)\frac{\partial^2 u_{[k,r]}}{\partial x\partial z}+C_{55}^{\{i\}}\frac{\partial^2 w_{[k,r]}}{\partial x^2}+C_{33}^{\{i\}}\frac{\partial^2 w_{[k,r]}}{\partial z^2}+e_5^{\{i\}}\frac{\partial^2 \phi_{[k,r]}}{\partial x^2}+e_3^{\{i\}}\frac{\partial^2 \phi_{[k,r]}}{\partial z^2}-\beta_3^{\{i\}}\frac{\partial T_{[k,r]}}{\partial z}=0\\
&\left(e_5^{\{i\}}+e_1^{\{i\}}\right)\frac{\partial^2 u_{[k,r]}}{\partial x\partial z}+e_5^{\{i\}}\frac{\partial^2 w_{[k,r]}}{\partial x^2}+e_3^{\{i\}}\frac{\partial^2 w_{[k,r]}}{\partial z^2}-\eta_1^{\{i\}}\frac{\partial^2 \phi_{[k,r]}}{\partial x^2}-\eta_3^{\{i\}}\frac{\partial^2 \phi_{[k,r]}}{\partial z^2}+p_3^{\{i\}}\frac{\partial T_{[k,r]}}{\partial z}=0\\
&\lambda_x^{\{i\}}\frac{\partial^2 T_{[k,r]}}{\partial x^2}+\lambda_z^{\{i\}}\frac{\partial^2 T_{[k,r]}}{\partial z^2}=0
\end{aligned}
\tag{23}
$$

As the two adjacent laminae are perfectly bonded, the continuity conditions $[[u,w]]=0$, $[[\phi]]=0$, and $[[T]]=0$ are satisfied a priori. The continuity conditions of transverse stresses are as follows:

$$
\begin{aligned}
&C_{13}^{\{i\}}\frac{\partial u_{[k,F_i]}}{\partial x}+C_{33}^{\{i\}}\frac{\partial w_{[k,F_i]}}{\partial z}+e_3^{\{i\}}\frac{\partial \phi_{[k,F_i]}}{\partial z}-\beta_3^{\{i\}}T_{[k,F_i]}\\
&\quad=C_{13}^{\{i+1\}}\frac{\partial u_{[k,F_i]}}{\partial x}+C_{33}^{\{i+1\}}\frac{\partial w_{[k,F_i]}}{\partial z}+e_3^{\{i+1\}}\frac{\partial \phi_{[k,F_i]}}{\partial z}-\beta_3^{\{i+1\}}T_{[k,F_i]}
\end{aligned}
\tag{24}
$$

$$
C_{55}^{\{i\}}\left(\frac{\partial u_{[k,F_i]}}{\partial z}+\frac{\partial w_{[k,F_i]}}{\partial x}\right)+e_5^{\{i\}}\frac{\partial \phi_{[k,F_i]}}{\partial x}=C_{55}^{\{i+1\}}\left(\frac{\partial u_{[k,F_i]}}{\partial z}+\frac{\partial w_{[k,F_i]}}{\partial x}\right)+e_5^{\{i+1\}}\frac{\partial \phi_{[k,F_i]}}{\partial x}
\tag{25}
$$

Table 2
Material properties of the graphite-epoxy and PZT-5A layers

Material properties	C_{11} (GPa)	C_{22} (GPa)	C_{33} (GPa)	C_{12} (GPa)	C_{13} (GPa)	C_{23} (GPa)	C_{44} (GPa)	C_{55} (GPa)	C_{66} (GPa)
Gr/Ep 0°	183.44	11.662	11.662	4.363	4.363	3.918	2.870	7.170	7.170
Gr/Ep 90°	11.662	183.44	11.662	4.363	3.918	4.363	7.170	2.870	7.170
PZT-5A	99.201	99.201	86.856	54.016	50.778	50.778	21.100	21.100	22.593

	β_1 (10^5 Pa K^{-1})	β_2 (10^5 Pa K^{-1})	β_3 (10^5 Pa K^{-1})
Gr/Ep 0°	2.000	3.506	3.506
Gr/Ep 90°	3.506	2.000	3.506
PZT-5A	3.314	3.314	3.260

	e_1 (C m^{-2})	e_2 (C m^{-2})	e_3 (C m^{-2})	e_4 (C m^{-2})	e_5 (C m^{-2})
Gr/Ep 0°	0	0	0	0	0
Gr/Ep 90°	0	0	0	0	0
PZT-5A	−7.209	−7.209	15.118	12.322	12.322

	η_1 (10^{-10} F/m)	η_2 (10^{-10} F/m)	η_3 (10^{-10} F/m)
Gr/Ep 0°	153.0	153.0	153.0
Gr/Ep 90°	153.0	153.0	153.0
PZT-5A	153.0	153.0	150.0

	p_1 (C m^{-2} K^{-1})	p_2 (C m^{-2} K^{-1})	p_3 (C m^{-2} K^{-1})
Gr/Ep 0°	0	0	0
Gr/Ep 90°	0	0	0
PZT-5A	0	0	0.0007

	κ_1 (W m^{-1} K^{-1})	κ_2 (W m^{-1} K^{-1})	κ_3 (W m^{-1} K^{-1})
Gr/Ep 0°	1.5	0.5	0.5
Gr/Ep 90°	0.5	1.5	0.5

Table 3
Convergence behaviour and deflection, normal stress, and electrical potential distribution through thickness of the hybrid laminate in Example 2 under sinusoidal thermal load ($\bar{w} = \frac{w}{a\alpha_0 T_0}$, $\bar{\sigma}_x = \frac{\sigma_x}{C_0\alpha_0 T_0}$, $\bar{\phi} = \frac{e_0\phi}{C_0 a\alpha_0 T_0}$, where $C_0 = 99.201$ Gpa, $e_0 = 7.209\ \mathrm{C\ m^{-2}}$, $\alpha_0 = 1.5\times10^{-6}\ \mathrm{K^{-1}}$ are representative moduli of PZT-5A.)

a/H	Mesh	$\bar{w}$		$\bar{\sigma}_x$						$\bar{\phi}\times10^5$
		$z=0$	$z=H$	$z=0$	$z=0.4H$	$z=0.4H$	$z=0.8H$	$z=0.8H$	$z=H$	$z=0.9H$
100	7	13.168	13.243	0.3306	1.3775	−0.6407	−1.3002	0.3338	0.2645	−2.8060
	9	13.284	13.360	0.3538	1.3400	−0.6428	−1.3058	0.2967	0.2140	−2.8324
	11	13.402	13.477	0.3211	1.3668	−0.6413	−1.3008	0.3298	0.2603	−2.8064
	13	13.436	13.511	0.3382	1.3438	−0.6426	−1.3046	0.3046	0.2264	−2.8237
	15	13.476	13.552	0.3187	1.3610	−0.6416	−1.3012	0.3269	0.2565	−2.8080
10	7	1.0849	1.8266	0.3663	1.2886	−0.6348	−1.2907	0.3757	0.3327	−28.766
	9	1.0883	1.8328	0.3905	1.2750	−0.6349	−1.2976	0.3191	0.3067	−28.323
	11	1.0870	1.8301	0.3766	1.2748	−0.6351	−1.2926	0.3585	0.3270	−28.576
	13	1.0857	1.8293	0.3833	1.2733	−0.6352	−1.2963	0.3322	0.3056	−28.574
6	7	0.3738	1.5788	0.4525	1.1571	−0.6231	−1.2785	0.4134	0.4275	−49.758
	9	0.3737	1.5826	0.4805	1.1594	−0.6222	−1.2857	0.3514	0.4199	−48.479
	11	0.3731	1.5813	0.4655	1.1585	−0.6223	−1.2818	0.3793	0.4377	−48.440
	13	0.3725	1.5808	0.4777	1.1520	−0.6228	−1.2838	0.3687	0.4167	−49.112
4	7	0.0912	1.6316	0.5769	0.9872	−0.5983	−1.2618	0.4336	0.5871	−78.306
	9	0.0921	1.6332	0.6208	0.9901	−0.5977	−1.2673	0.3879	0.5858	−77.367
	11	0.0907	1.6345	0.5858	1.0016	−0.5970	−1.2658	0.3950	0.6044	−75.766
	13	0.0912	1.6346	0.6195	0.9847	−0.5980	−1.2663	0.3945	0.5926	−77.418

Table 4
Convergence behaviour and deflection, normal stress, and electrical potential distribution through thickness of the hybrid laminate in Example 2 under uniform thermal load ($\bar{w} = \frac{w}{a\alpha_0 T_0}$, $\bar{\sigma}_x = \frac{\sigma_x}{C_0\alpha_0 T_0}$, $\bar{\phi} = \frac{e_0\phi}{C_0 a\alpha_0 T_0}$, where $C_0 = 99.201$ Gpa, $e_0 = 7.209\ \mathrm{C\ m^{-2}}$, $\alpha_0 = 1.5\times10^{-6}\ \mathrm{K^{-1}}$ are representative moduli of PZT-5A.)

a/H	Mesh	$\bar{w}$		$\bar{\sigma}_x$						$\bar{\phi}\times10^5$
		$z=0$	$z=H$	$z=0$	$z=0.4H$	$z=0.4H$	$z=0.8H$	$z=0.8H$	$z=H$	$z=0.9H$
20	11	1.8377	2.2191	0.7127	1.0279	−0.6628	−1.3695	−0.0938	−0.4258	−16.514
	13	1.9134	2.2951	0.7691	1.2418	−0.6469	−1.3384	0.0719	0.0624	−14.723
	15	1.9300	2.3115	0.7915	1.1331	−0.6557	−1.3544	0.0060	−0.2811	−15.974
	17	1.9664	2.3472	0.7823	1.2420	−0.6478	−1.3417	0.0608	−0.1170	−15.139
	19	1.9815	2.3622	0.8090	1.2131	−0.6508	−1.3470	0.0382	−0.2067	−15.665
	21	1.9973	2.3786	0.8032	1.2293	−0.6485	−1.3430	0.0516	−0.1302	−15.211
10	7	0.6748	1.4327	0.5172	0.8999	−0.6707	−1.3842	−0.1737	−0.5996	−35.074
	11	0.8090	1.5709	0.7014	1.1135	−0.6574	−1.3504	0.0248	−0.2814	−32.527
	15	0.8610	1.6198	0.7240	1.2504	−0.6492	−1.3386	0.0974	−0.1593	−31.319
	19	0.8766	1.6347	0.7102	1.2678	−0.6478	−1.3354	0.1199	−0.1406	−31.268
5	9	0.0601	1.5783	0.6155	1.1847	−0.6456	−1.3150	0.2270	0.2209	−54.765
	13	0.0836	1.6048	0.6638	1.1567	−0.6481	−1.3172	0.2021	0.2069	−55.868
	17	0.0928	1.6101	0.6676	1.1743	−0.6478	−1.3151	0.2245	0.1751	−57.761
	21	0.0969	1.6131	0.6822	1.1763	−0.6478	−1.3149	0.2277	0.1699	−58.275

Similarly, the continuity condition of the normal component of the electric displacement and the heat flux are

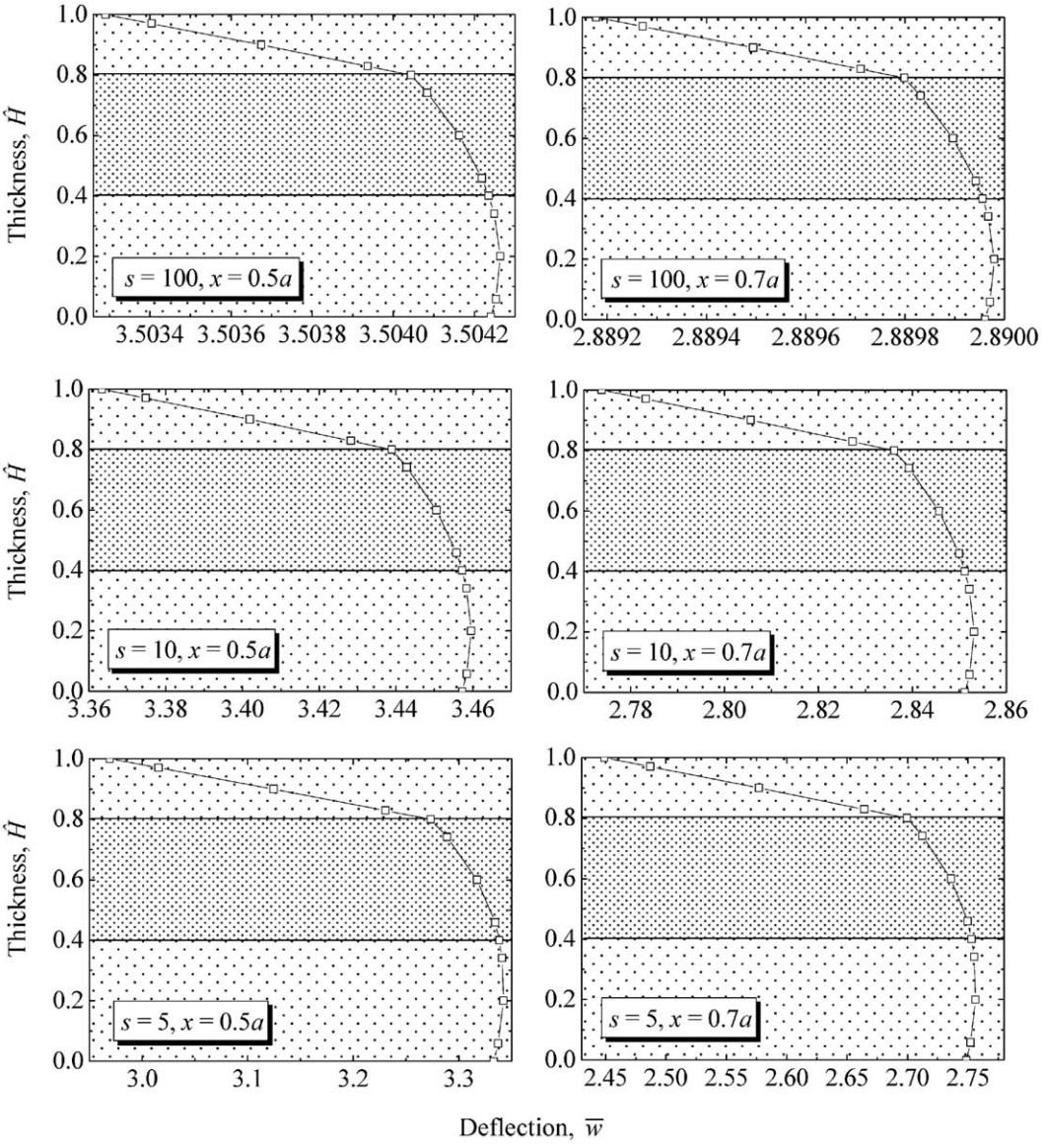

Fig. 2. Deflection distribution through thickness ($\bar{w} = \frac{10wH^2}{a^2 d_T \phi_0}$, where $d_T = 374 \times 10^{-12}$ m/V).

$$e_1^{\{i\}} \frac{\partial u_{[k,F_i]}}{\partial x} + e_3^{\{i\}} \frac{\partial w_{[k,F_i]}}{\partial z} - \eta_3^{\{i\}} \frac{\partial \phi_{[k,F_i]}}{\partial z} + p_3^{\{i\}} T_{[k,F_i]} = e_1^{\{i+1\}} \frac{\partial u_{[k,F_i]}}{\partial x} + e_3^{\{i+1\}} \frac{\partial w_{[k,F_i]}}{\partial z} - \eta_3^{\{i+1\}} \frac{\partial \phi_{[k,F_i]}}{\partial z} + p_3^{\{i+1\}} T_{[k,F_i]} \tag{26}$$

$$-\kappa_{13}^{\{i\}} \frac{\partial T_{[k,F_i]}}{\partial x} - \kappa_{33}^{\{i\}} \frac{\partial T_{[k,F_i]}}{\partial z} = -\kappa_{13}^{\{i+1\}} \frac{\partial T_{[k,F_i]}}{\partial x} - \kappa_{33}^{\{i+1\}} \frac{\partial T_{[k,F_i]}}{\partial z} \tag{27}$$

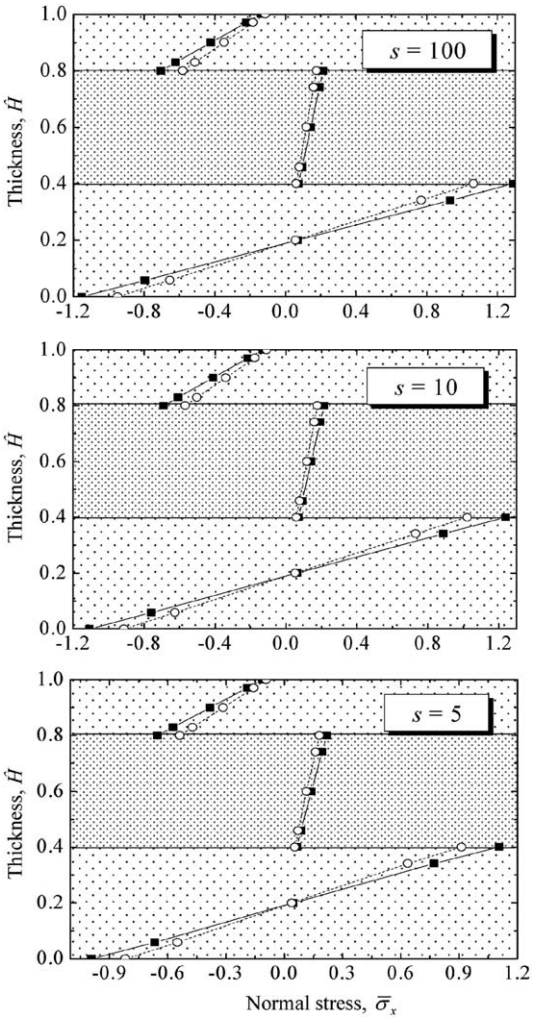

Fig. 3. Distribution of in-plane normal stress through thickness ($\bar{\sigma}_x = \frac{\sigma_x H}{10E_T d_T \phi_0}$, where $E_T = 10.3$ GPa and $d_T = 374 \times 10^{-12}$ m/V). (–■–) for $x = 0.5a$, and (–○–) for $x = 0.7a$.

In particular, the derivative in the z-direction is discretised within the corresponding lamina in Eqs. (24)–(27), for example, $\kappa_{33}^{\{i\}} \frac{\partial T_{[k,F_i]}}{\partial z}$ in the left of Eq. (27) is discretised within the ith lamina, and $\kappa_{33}^{\{i+1\}} \frac{\partial T_{[k,F_i]}}{\partial z}$ within the $i+1$th lamina.

3. Numerical examples

The proposed method has been tested for a few selected plate problems. In this section, the numerical results for these problems are presented, and compared with the available analytical solutions as well as the numerical solutions.

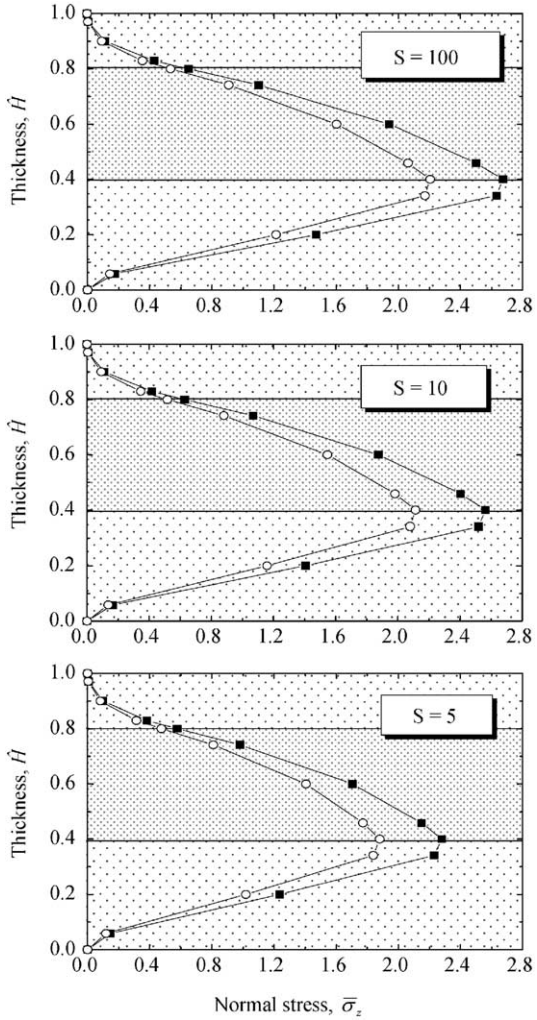

Fig. 4. Distribution of transverse normal stress through thickness ($\bar{\sigma}_z = \frac{\sigma_z a^2}{HE_T d_T \phi_0}$, where $E_T = 10.3$ GPa and $d_T = 374 \times 10^{-12}$ m/V). (–■–) for $x = 0.5a$, and (–○–) for $x = 0.7a$.

3.1. Example 1: Piezoelectric panel under cylindrical bending with electrostatic excitation

The first example is taken from Dube et al. (1996). It is an infinitely long flat panel, with two ends in the x-direction of the panel simply supported, electrically earthed and maintained at a reference temperature, i.e.

- Simply supported at $x = 0$ and a : $\sigma_x = \tau_{xy} = w = 0$ (28)
- Electrically grounded at $x = 0$ and a : $\phi = 0$ (29)
- Fixed temperature at $x = 0$ and a : $T = 0$ (30)

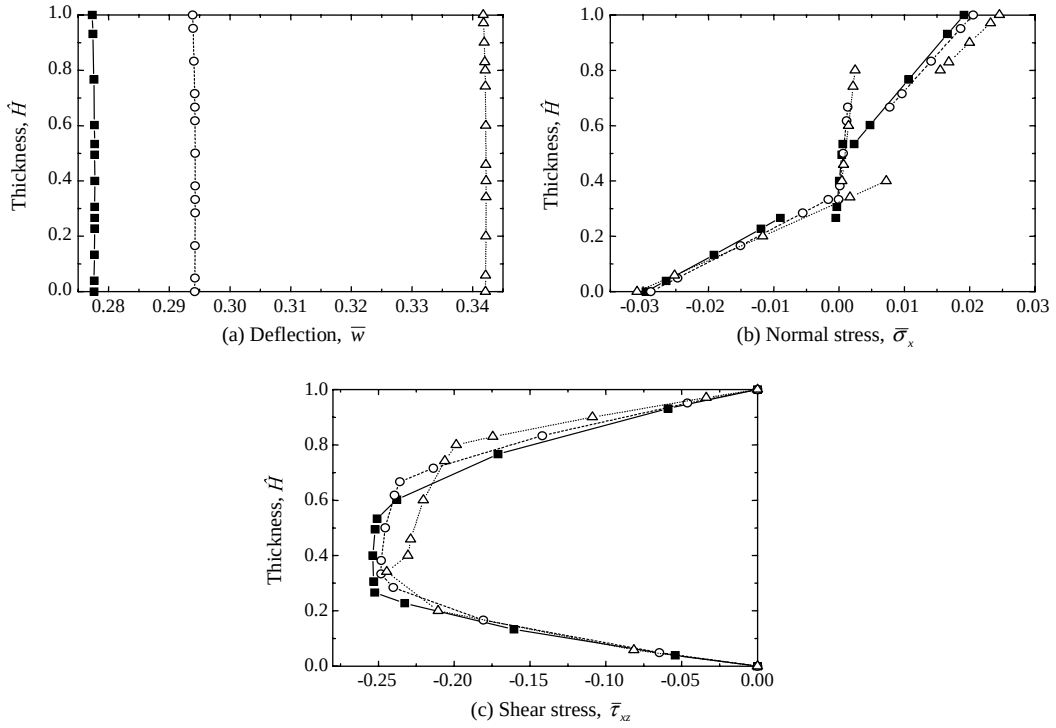

Fig. 5. Hybrid thin laminated plates with clamp-support in Example 4 under mechanical load ($\bar{w} = \frac{100wE_T H^3}{a^4 q_0}$, $\bar{\sigma}_x = \frac{10\sigma_x H^2}{a^2 q_0}$, $\bar{\tau}_{xz} = \frac{\tau_{xz} H}{a q_0}$, where $E_T = 10.3$ GPa). $s = 100/3$, (–■–) $\zeta = 4{:}4{:}7$, (--○--) $\zeta = 1{:}1{:}1$, ($\cdots\triangle\cdots$) $\zeta = 2{:}2{:}1$.

The simply supported conditions that are given in Eq. (28) can be discretised as

$$w_{[1\text{ or }J,r]} = 0 \tag{31}$$

$$C_{11}^{\{i\}} \frac{\partial u_{[1,r]}}{\partial x} + C_{13}^{\{i\}} \frac{\partial w_{[1,r]}}{\partial z} + e_1^{\{i\}} \frac{\partial \phi_{[1,r]}}{\partial z} - \beta_1^{\{i\}} T_{[1,r]} = 0 \text{ at } x = 0, \quad z = z_r \tag{32}$$

or

$$C_{11}^{\{i\}} \frac{\partial u_{[J,r]}}{\partial x} + C_{13}^{\{i\}} \frac{\partial w_{[J,r]}}{\partial z} + e_1^{\{i\}} \frac{\partial \phi_{[J,r]}}{\partial z} - \beta_1^{\{i\}} T_{[J,r]} = 0 \text{ at } x = a, \quad z = z_r \tag{33}$$

where $i = 1, 2, \ldots, N_L$, $r = 1, 2, \ldots, F_i$.

The electric and thermal conditions that are expressed in Eqs. (29) and (30) can be described as follows

$$\phi_{[1\text{ or }J,r]} = 0 \tag{34}$$

$$T_{[1\text{ or }J,r]} = 0 \tag{35}$$

The lateral surfaces are traction-free, i.e.

$$\sigma_z = \tau_{xz} = \tau_{yz} = 0 \text{ at } z = 0 \text{ and } H \tag{36}$$

and they are kept at $T = 0$. The bottom surface ($z = 0$) is electrically grounded, i.e., $\phi = 0$. The top surface ($z = H$) is loaded with a sinusoidal electric field

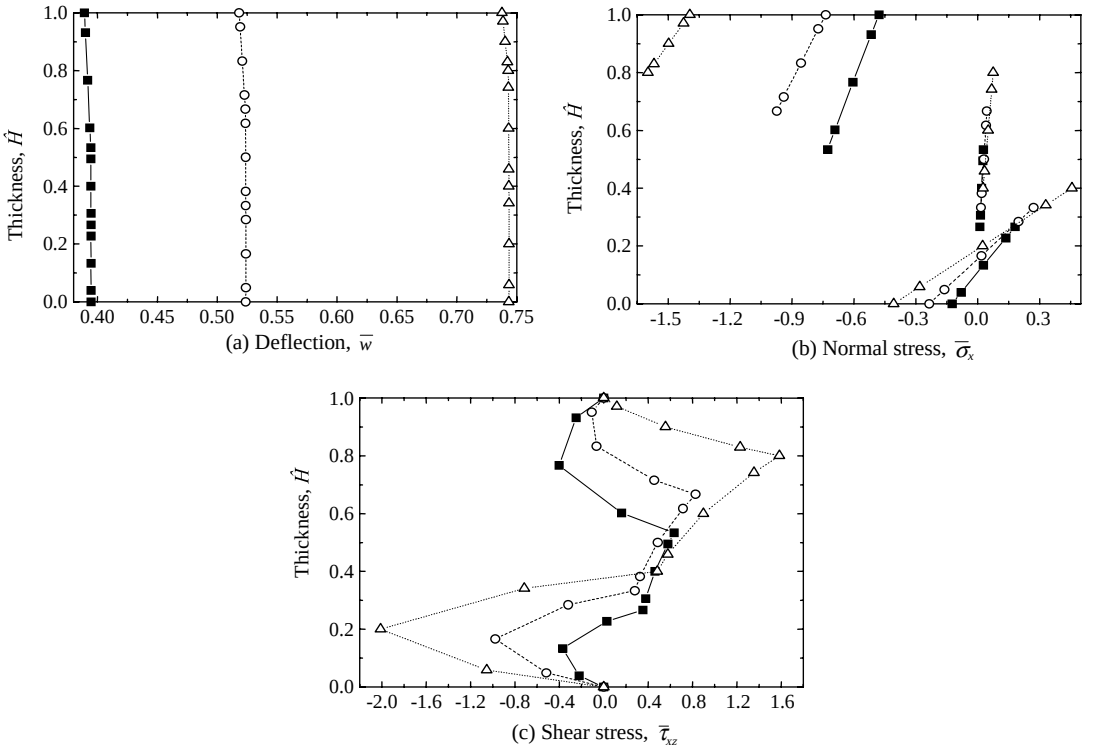

Fig. 6. Hybrid thin laminated plates with clamp-support in Example 4 under electrical load ($\bar{w} = \frac{100wE_TH^3}{a^4q_0}$, $\bar{\sigma}_x = \frac{10\sigma_xH^2}{a^2q_0}$, $\bar{\tau}_{xz} = \frac{\tau_{xz}H}{aq_0}$, where $E_T = 10.3$ GPa). $s = 100/3$, (–■–) $\zeta = 4{:}4{:}7$, (--○--) $\zeta = 1{:}1{:}1$, ($\cdots\triangle\cdots$) $\zeta = 2{:}2{:}1$.

$$\phi = \phi_0 \sin(\pi x/a) \tag{37}$$

where ϕ_0 is a given constant.

The discrete forms of the bottom surface conditions (see Eq. (36)) at $x = x_k$, $z = 0$ can be written as

$$C_{13}^{\{1\}}\frac{\partial u_{[k,1]}}{\partial x} + C_{33}^{\{1\}}\frac{\partial w_{[k,1]}}{\partial z} + e_3^{\{1\}}\frac{\partial \phi_{[k,1]}}{\partial z} - \beta_3^{\{1\}}T_{[k,1]} = 0 \tag{38}$$

$$C_{55}^{\{1\}}\left(\frac{\partial u_{[k,1]}}{\partial z} + \frac{\partial w_{[k,1]}}{\partial x}\right) + e_5^{\{1\}}\frac{\partial \phi_{[k,1]}}{\partial x} = 0 \tag{39}$$

and on the top surface, i.e. $x = x_k$, $z = H$, the discrete conditions are

$$C_{13}^{\{1\}}\frac{\partial u_{[k,F_{N_L}]}}{\partial x} + C_{33}^{\{1\}}\frac{\partial w_{[k,F_{N_L}]}}{\partial z} + e_3^{\{1\}}\frac{\partial \phi_{[k,F_{N_L}]}}{\partial z} - \beta_3^{\{1\}}T_{[k,F_{N_L}]} = 0 \tag{40}$$

$$C_{55}^{\{1\}}\left(\frac{\partial u_{[k,F_{N_L}]}}{\partial z} + \frac{\partial w_{[k,F_{N_L}]}}{\partial x}\right) + e_5^{\{1\}}\frac{\partial \phi_{[k,F_{N_L}]}}{\partial x} = 0 \tag{41}$$

The prescribed surface temperature condition is

$$T_{[k,1\text{ or }F_{N_L}]} = 0 \tag{42}$$

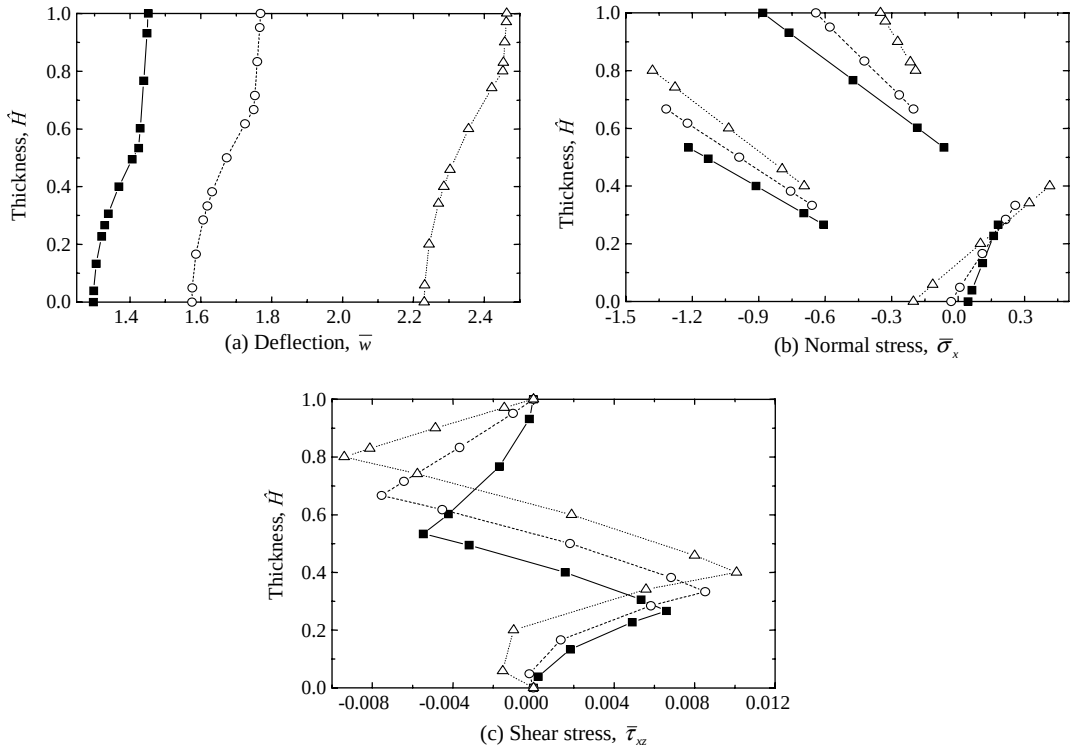

Fig. 7. Hybrid thin laminated plates with clamp-support in Example 4 under thermal load ($\bar{w} = \frac{100wE_TH^3}{a^4q_0}$, $\bar{\sigma}_x = \frac{10\sigma_xH^2}{a^2q_0}$, $\bar{\tau}_{xz} = \frac{\tau_{xz}H}{aq_0}$, where $E_T = 10.3$ GPa). $s = 100/3$, (–■–) $\zeta = 4{:}4{:}7$, (--○--) $\zeta = 1{:}1{:}1$, (···△···) $\zeta = 2{:}2{:}1$.

The surface conditions of the electric field are

$$\phi_{[k,1]} = 0 \text{ at } z = 0 \tag{43}$$

$$\phi_{[k,F_{N_L}]} = \phi_0 \sin(\pi x_k/a) \text{ at } z = H \tag{44}$$

Both the edge-support conditions and lateral surface conditions do not vary along the longitudinal direction.

The material properties of the pate are given as follows (Dube et al., 1996):

$$C_{11} = C_{22} = 74.1 \text{ GPa}, \quad C_{33} = 83.6 \text{ GPa}, \quad C_{44} = C_{55} = 13.17 \text{ GPa},$$
$$C_{66} = 14.45 \text{ GPa}, \quad C_{12} = 45.2 \text{ GPa}, \quad C_{13} = C_{23} = 39.3 \text{ GPa},$$
$$e_1 = e_2 = -0.160 \text{ C m}^{-2}, \quad e_3 = 0.347 \text{ C m}^{-2}, \quad e_4 = 0, \; e_5 = -0.138 \text{ C m}^{-2},$$
$$\eta_1 = \eta_2 = 82.5 \times 10^{-12} \text{ C}^2 \text{ N}^{-1} \text{ m}^{-2}, \quad \eta_3 = 90.2 \times 10^{-12} \text{ C}^2 \text{ N}^{-1} \text{ m}^{-2},$$
$$\beta_1 = \beta_2 = 0.621 \times 106 \text{ N K}^{-1} \text{ m}^{-2}, \quad \beta_3 = 0.551 \times 106 \text{ N K}^{-1} \text{ m}^{-2},$$
$$p_3 = -2.94 \times 10^{-6} \text{ C K}^{-1} \text{ m}^{-2}, \quad \lambda_z/\lambda_x = 1.5,$$
$$\alpha_x = 4.396 \times 10^{-6} \text{ K}^{-1}, \quad d_1 = -3.9238 \times 10^{-12} \text{ C N}^{-1}, \quad Y_x = 42.785 \text{ GPa}.$$

The computed results for this example are shown in Table 1. Rapid convergence of the present results is attained. The dimensionless parameters, $\bar{w}$, $\bar{\sigma}_x$, $\bar{\sigma}_y$ and $\bar{\phi}$, are compared to the results of Dube et al. (1996). They are in excellent agreement.

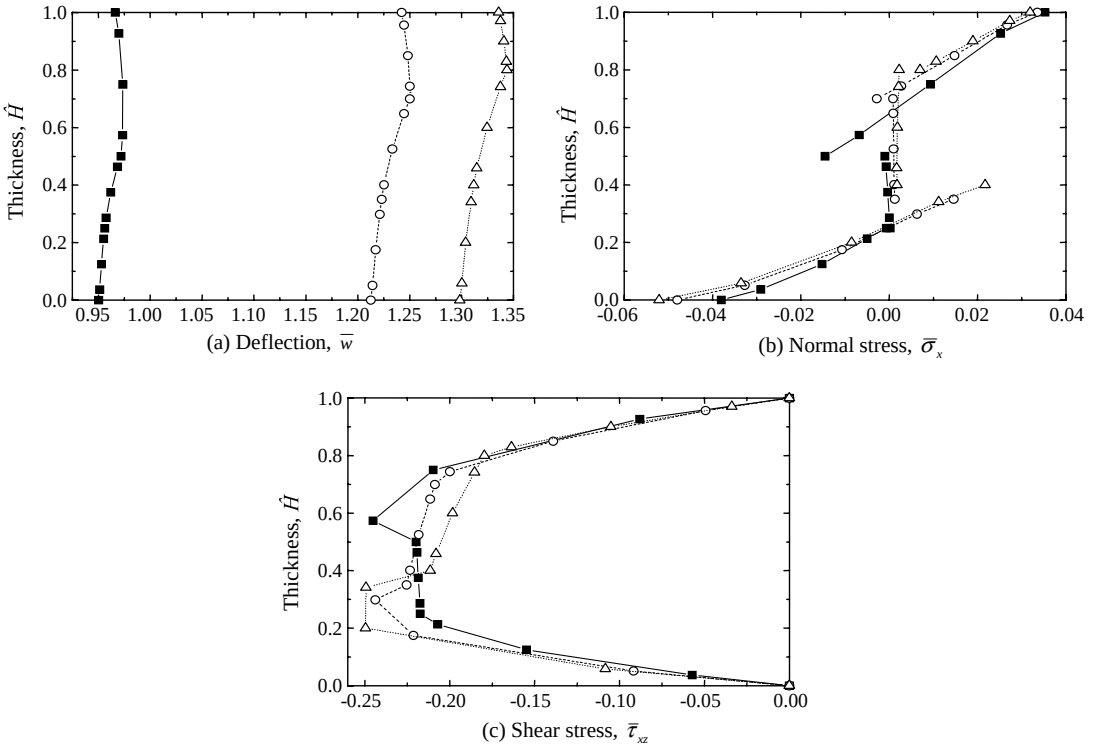

Fig. 8. Hybrid thick laminated plates with clamp-support in Example 4 under mechanical load ($\bar{w} = \frac{100wE_T H^3}{a^4 q_0}$, $\bar{\sigma}_x = \frac{10\sigma_x H^2}{a^2 q_0}$, $\bar{\tau}_{xz} = \frac{\tau_{xz} H}{a q_0}$, where $E_T = 10.3$ GPa). $s = 5$, (–■–) $\zeta = 1{:}1{:}2$, (--○--) $\zeta = 7{:}7{:}6$, (···△···) $\zeta = 2{:}2{:}1$.

3.2. Example 2: Plate containing a piezoelectric lamina poled in thickness direction

The second example considered is a three-layered cross-ply plate (Vel and Batra, 2003). The two bottom layers are made of Gr/Ep material and the top is a thickness-poled PZT-5A layer. The fibres are oriented in parallel and perpendicular to the x-axis in the bottom and middle layers, i.e. 0° Gr/Ep and 90° Gr/Ep. Each Gr/Ep lamina is of thickness 0.4H. The PZT-5A layer is half the thickness of Gr/Ep lamina, i.e. 0.2H.

The edge at $x = 0$ is clamped such that

$$u = v = w = 0 \tag{45}$$

and they can be cast in the following DQ discrete form

$$u_{[1 \text{ or } J,r]} = w_{[1 \text{ or } J,r]} = 0 \tag{46}$$

The edge at $x = a$ is simply-supported, as described in Eq. (28). Both edges are electrically grounded as in Eq. (29), and maintained at the reference temperature, as described in Eq. (30). The two lateral surfaces are also electrically grounded. The temperature at the bottom surface is kept at $T = 0$, and the top surface is thermally loaded with a sinusoidal temperature at $z = H$, i.e.

$$T = T_0 \sin(\pi x/a) \tag{47}$$

where T_0 is a given constant. The thermal load can be expressed in the following DQ form

$$T_{[k,F_{N_L}]} = T_0 \sin(\pi x_k/a) \text{ or } T_0 \tag{48}$$

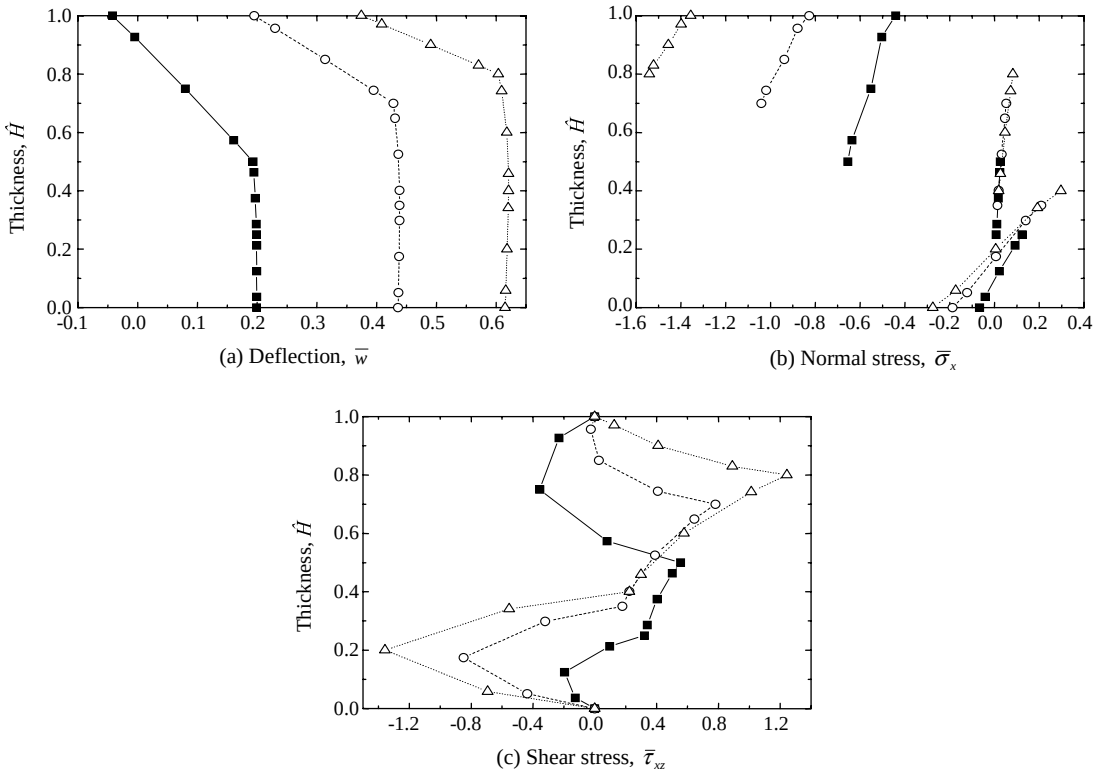

Fig. 9. Hybrid thick laminated plates with clamp-support in Example 4 under electrical load ($\bar{w} = \frac{100wE_TH^3}{a^4q_0}$, $\bar{\sigma}_x = \frac{10\sigma_xH^2}{a^2q_0}$, $\bar{\tau}_{xz} = \frac{\tau_{xz}H}{aq_0}$, where $E_T = 10.3$ GPa). $s = 5$, (–■–) $\zeta = 1{:}1{:}2$, (--○--) $\zeta = 7{:}7{:}6$, ($\cdots\triangle\cdots$) $\zeta = 2{:}2{:}1$.

The interface at the middle Gr/Ep and PZT-5A layer is also electrically grounded. Material properties that are taken from Vel and Batra (2003) are listed in Table 2.

Deflection $\bar{w}$, normal stress $\bar{\sigma}_x$ and electrical potential $\bar{\phi}$ at the central point of the panel under the two types of thermal loads described in Eq. (18) are presented in Tables 3 and 4. The results show a rapid convergence trend. It can also be seen that when the laminated plate is very thin, for example $a/H = 100$, the deflections at the two lateral surfaces are almost identical. As a/H increases, the difference in the deflections between the two lateral surfaces becomes evident, especially when a/H is 4 in Table 3 and a/H is 5 in Table 4. In fact, at these ratios the deflection at the bottom surface is quite small compared to that at the top surface. The maximum normal stresses occur at the interfaces. The stress at the interface between the Gr/Ep and PZT-5A layers is more pronounced than between the two Gr/Ep layers, except for the case in which $a/H = 100$.

3.3. Example 3: Laminated plates under an electrical load

The configuration of this plate example is the same as that described in the previous example, except that the two edges are now simply-supported and under an electrical load. The simply-supported condition has been described in Eq. (28) and the electrical load in Eq. (37). The material properties used in this example were given in the previous example.

The distributions of the transverse displacement and normal stresses through the thickness at the plate central point (i.e. $x = 0.5a$) and $x = 0.7a$ are plotted in Figs. 2–4. Fig. 2 shows that the transverse displace-

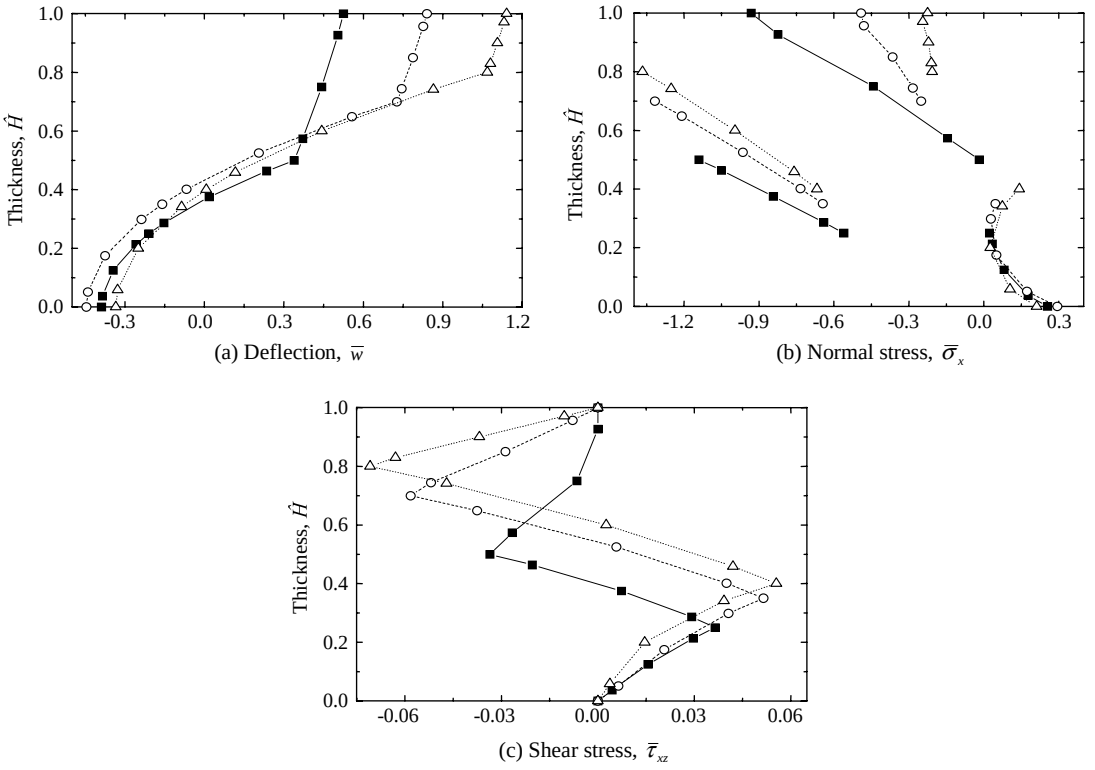

Fig. 10. Hybrid thick laminated plates with clamp-support in Example 4 under thermal load ($\bar{w} = \frac{100wE_T H^3}{a^4 q_0}$, $\bar{\sigma}_x = \frac{10\sigma_x H^2}{a^2 q_0}$, $\bar{\tau}_{xz} = \frac{\tau_{xz} H}{a q_0}$, where $E_T = 10.3$ GPa). $s = 5$, (–■–) $\zeta = 1{:}1{:}2$, (--○--) $\zeta = 7{:}7{:}6$, ($\cdots\triangle\cdots$) $\zeta = 2{:}2{:}1$.

ment is distributed linearly in the PZT layer (top layer). However, the transverse displacement in the two Gr/Ep layers is distributed nonlinearly. The deflection at the bottom surface is larger than that at the top surface. In Fig. 3, the in-plane normal stress $\bar{\sigma}_x$ is linearly distributed in both the PZT and Gr/Ep layers for all thicknesses. The distributions of transverse normal stress $\bar{\sigma}_z$ are shown in Fig. 4. As expected, the transverse normal stresses $\bar{\sigma}_z$ for all cases are nonlinearly distributed.

3.4. Example 4: Laminated plate under mechanical, electrical and thermal loads

We consider a three-layered laminated plate stacked with two bottom Gr/Ep layers and a top layer of one thickness-poled PZT-5A. The stacking sequence is 0° Gr/Ep (bottom), 90° Gr/Ep (middle) and PZT-5A (top). We vary the thickness ratio of each layer as follows: (a) for $s = 100/3$, the thickness ratios ζ for 0° Gr/Ep, 90° Gr/Ep and PZT-5A are 4:4:7, 1:1:1, and 2:2:1; and (b) for $s = 5$, the thickness ratios ζ are 1:1:2, 7:7:6, and 2:2:1.

The plate is considered with two edges clamped (Eqs. (45) and (46)), electrically grounded (Eq. (29)) and maintained at the reference temperature (Eq. (30)). The bottom surface is free from loading, but the top surface is mechanically loaded by a sinusoidal normal stress at $z = H$, i.e.

$$\sigma_z = q_0 \sin(\pi x/a) \text{ and } \tau_{xz} = \tau_{yz} = 0 \tag{49}$$

where q_0 is a given constant. The discrete top surface conditions at ($x = x_k, z = H$) are similar to Eqs. (40) and (41), except in Eq. (40) the part in the right-side has to change to $q_0 \sin(\pi x_k/\mathrm{a})$ or be electrically loaded,

as described in Eq. (37), or thermally loaded as described in Eq. (47). The interfacial conditions that were employed in Example 2 are used. The material properties that were used in Example 2 are also adopted in this calculation.

Figs. 5–7 show the variation of deflection, normal in-plane stress and transverse shear stress for $s = 100/3$ with three thickness layer ratios ζ subject to the mechanical, electrical and thermal loading conditions. In this case, we select three thickness layer ratios, 4:4:7, 1:1:1 and 2:2:1, to illustrate the variations under the three different types of loading condition. Under the same loading conditions but with $s = 5$, the variations of deflection, normal in-plane stress and transverse shear stress for the three thickness layer ratios ζ are given in Figs. 8–10. The thickness layer ratios considered are 1:1:2, 7:7:6 and 2:2:1. Comparing the responses of the laminated panel under different loads, it is clear that non-uniform deformations among the layers of the laminated panel occur under the thermal load. This is especially obvious for the thicker laminate, in which the top PZT layer deflects more. When $s = 5$, the electrical load furnishes a larger deflection in the bottom layer than the top layer. The maximum stress component $\bar{\sigma}_x$ of the panel is more pronounced for the thinner top PZT layer than the thicker layer. It is expected that the stress distributions vary for different loading conditions. A similar occurs with the shear stress $\bar{\tau}_{xz}$. There is a larger shear stress for the thinner top PZT layer, except for the cases under the mechanical loads where the thickness of the top PZT layer does not make much difference. When the plate is under an electrical load, the maximum $\bar{\sigma}_x$ occurs at the interface between the mid Gr/Ep layer and the top PZT layer. However this is not the same for the maximum $\bar{\tau}_{xz}$ even though there is a large shear stress at the interface. When the plate is subjected to thermal load, these two maximum values occur at the interface between the two top layers. It is worth noting that the jumps of normal stress $\bar{\sigma}_x$ along the interfaces, especially the interface of the two top laminae, are quite noticeable.

4. Conclusions

This paper has presented an analysis of the static behaviour of multilayered composite plates that are subject to thermo-piezoelectric-mechanical loading. The analysis was carried out using the three-dimensional equations of thermo-piezoelasticity and the differential quadrature (DQ) layerwise model. Numerical results were presented for plates with different combinations of boundary conditions, and were found to be comparable to the existing analytical solution. We also investigated the effects of the thermo-piezoelasticity of these problems. Some interesting phenomena were revealed. The piezoelectric panel showed different forms of mechanical behaviour than the homogenous plates. The transverse displacement of the piezoelectric panel was larger at the bottom surface than that at the top surface. The distributions of displacement and stresses for the piezoelectric laminate were quite consistent. Our study shows that at different locations along the width of the panels, the distribution trends for different thickness ratios s are similar. They are different only in their magnitude. This indicates that the transverse functions of the physical quantities are independent of x, but their magnitudes are functions of x.

References

Bert, C.W., Malik, M., 1996. Differential quadrature method in computational mechanics: a review. Appl. Mech. Rev. 49, 1–28.

Dube, G.P., Santosh, K., Dumir, P.C., 1996. Exact piezothermoelastic solution of simply-supported orthotropic flat panel in cylindrical bending. Int. J. Mech. Sci. 38, 1161–1177.

Han, J.B., Liew, K.M., 1997a. An eight-node curvilinear differential quadrature formulation for Reissner/Mindlin plates. Comput. Meth. Appl. Mech. Eng. 141, 265–280.

Han, J.B., Liew, K.M., 1997b. Numerical differential quadrature method for Reissner/Mindlin plates on two-parameter foundations. Int. J. Mech. Sci. 39, 977–990.

Han, J.B., Liew, K.M., 1997c. Analysis of moderately thick circular plates using differential quadrature method. J. Eng. Mech. ASCE 123, 1247–1252.

Heyliger, P.R., 1994. Static behavior of laminated elastic/piezoelectric plates. AIAA J. 32, 2481–2484.
Heyliger, P.R., 1997. Exact solutions for simply supported laminated piezoelectric plates. J. Appl. Mech. 64, 299–306.
Liew, K.M., Han, J.B., Xiao, Z.M., 1996a. Differential quadrature method for thick symmetric cross-ply laminates with first-order shear flexibility. Int. J. Solids Struct. 33, 2647–2658.
Liew, K.M., Han, J.B., Xiao, Z.M., Du, H., 1996b. Differential quadrature method for Mindlin plates on Winkler foundations. Int. J. Mech. Sci. 38, 405–421.
Liew, K.M., Teo, T.M., 1998. Modeling via differential quadrature method. Three-dimensional solutions for rectangular plates. Comput. Meth. Appl. Mech. Eng. 159, 369–381.
Liew, K.M., Han, J.B., 1997. A four-node differential quadrature method for straight-sided quadrilateral Reissner/Mindlin plates. Commun. Num. Meth. Eng. 13, 62–73.
Liew, K.M., Teo, T.M., 1999. Three-dimensional vibration analysis of rectangular plates based on differential quadrature method. J. Sound Vibr. 220, 577–599.
Liew, K.M., Teo, T.M., Han, J.B., 1999. Comparative accuracy of DQ and HDQ methods for three-dimensional vibration analysis of rectangular plates. Int. J. Num. Meth. Eng. 45, 1831–1848.
Liew, K.M., Liu, F.L., 2000. Differential quadrature method for vibration analysis of shear deformable annular sector plates. J. Sound Vibr. 230, 335–356.
Liew, K.M., Teo, T.M., Han, J.B., 2001. Three-dimensional static solutions of rectangular plates by variant differential quadrature method. Int. J. Mech. Sci. 43, 1611–1628.
Liew, K.M., Ng, T.Y., Zhang, Z.J., 2002. Differential quadrature-layerwise modeling technique for three-dimensional analysis of cross-ply laminated plates of various edge-supports. Comput. Meth. Appl. Mech. Eng. 191, 3811–3832.
Liew, K.M., Zhang, Z.J., Ng, T.Y., Reddy, J.N., 2004. Dynamic characteristics of elastic bonding in composite laminates a free vibration study. ASME J. Appl. Mech. 70, 860–870.
Liu, F.L., Liew, K.M., 1998a. Differential cubature method for static solutions of arbitrarily shaped thick plates. Int. J. Solids Struct. 35, 3655–3674.
Liu, F.L., Liew, K.M., 1998b. Static analysis of Mindlin plates by differential quadrature element method. ASME J. Appl. Mech. 65, 705–710.
Liu, F.L., Liew, K.M., 1999a. Free vibration analysis of Mindlin sector plates: numerical solutions by differential quadrature method. Comput. Meth. Appl. Mech. Eng. 177, 77–92.
Liu, F.L., Liew, K.M., 1999b. Differential quadrature method: a new approach for free vibration analysis of polar Mindlin plates having discontinuities. Comput. Meth. Appl. Mech. Eng. 179, 407–423.
Mindlin, R.D., 1974. Equations of high frequency vibrations of thermopiezoelectric crystal plates. Int. J. Solids Struct. 10, 625–637.
Nowacki, W., 1975. Thermoelasticity of anisotropic and piezoelectric bodies. In: Dynamic Problems of Thermoelasticity. Noordhoff, Leyden, Chapter 5.
Nowacki, W., 1978. Some general theorems of thermopiezoelectricity. J. Thermal Stresses 1, 171–182.
Pagano, N.J., 1970. Exact solutions for rectangular bidirectional composites and sandwich plates. J. Compos. Mater. 4, 20–34.
Ray, M.C., Rao, K.M., Samanta, B., 1992. Exact analysis of coupled electroelastic behaviour of a piezoelectric plate under cylindrical bending. Comput. Struct. 45, 667–677.
Ray, M.C., Rao, K.M., Samanta, B., 1993. Exact solution for static analysis of an intelligent structure under cylindrical bending. Comput. Struct. 47, 1031–1042.
Reddy, J.N., 2004. Mechanics of Laminated Composite Plates and Shells: Theory and Analysis, second ed. CRC Press, Boca Raton, FL.
Srinivas, S., Rao, A.K., 1970. Bending, vibration and buckling of simply supported thick orthotropic rectangular plates and laminates. Int. J. Solids Struct. 6, 1463–1481.
Teo, T.M., Liew, K.M., 1999a. Three-dimensional elasticity solutions to some orthotropic plate problems. Int. J. Solids Struct. 36, 5301–5326.
Teo, T.M., Liew, K.M., 1999b. A differential quadrature procedure for three-dimensional buckling analysis of rectangular plates. Int. J. Solids Struct. 36, 1149–1168.
Tiersten, H.F., 1971. On the nonlinear equations of thermoelectroelasticity. Int. J. Eng. Sci. 9, 587–604.
Vel, S.S., Batra, R.C., 2000. Cylindrical bending of laminated plates with distributed and segmented piezoelectric actuators/sensors. AIAA J. 38, 857–867.
Vel, S.S., Batra, R.C., 2003. Generalized plane strain thermopiezoelectric analysis of multilayered plates. J. Thermal Stresses 26, 353–377.
Xu, K.M., Noor, A.K., Tang, Y.Y., 1995. Three-dimensional solutions for coupled thermoelectroelastic response of multilayered plates. Comput. Meth. Appl. Mech. Eng. 126, 355–371.
Zhang, Z., Ng, T., Liew, K.M., 2003. Three-dimensional theory of elasticity for free vibration analysis of composite laminates via layerwise differential quadrature modeling. Int. J. Num. Meth. Eng. 57, 1819–1844.